

# Origin of Capacity Fading in Nano-Sized $\text{Co}_3\text{O}_4$ Electrodes: Electrochemical Impedance Spectroscopy Study

Jin-Gu Kang · Young-Dae Ko · Jae-Gwan Park · Dong-Wan Kim

Received: 26 August 2008 / Accepted: 11 September 2008 / Published online: 25 September 2008  
© to the authors 2008

**Abstract** Transition metal oxides have been suggested as innovative, high-energy electrode materials for lithium-ion batteries because their electrochemical conversion reactions can transfer two to six electrons. However, nano-sized transition metal oxides, especially  $\text{Co}_3\text{O}_4$ , exhibit drastic capacity decay during discharge/charge cycling, which hinders their practical use in lithium-ion batteries. Herein, we prepared nano-sized  $\text{Co}_3\text{O}_4$  with high crystallinity using a simple citrate-gel method and used electrochemical impedance spectroscopy method to examine the origin for the drastic capacity fading observed in the nano-sized  $\text{Co}_3\text{O}_4$  anode system. During cycling, AC impedance responses were collected at the first discharged state and at every subsequent tenth discharged state until the 100th cycle. By examining the separable relaxation time of each electrochemical reaction and the goodness-of-fit results, a direct relation between the charge transfer process and cycling performance was clearly observed.

**Keywords** Nano-sized  $\text{Co}_3\text{O}_4$  · Li-ion batteries · Capacity fading · Electrochemical impedance spectroscopy · Charge transfer reaction

## Introduction

The development of rechargeable lithium-ion batteries with higher specific capacity, higher power density, and longer cycle life is one of the key issues in the field of portable

energy storage devices. The nanostructuring of electrode materials has therefore recently attracted much attention due to the short transport length of both electron and lithium ions, higher electrode/electrolyte contact area, and better accommodation of the strain during cycling [1–3]. Especially, nano-sized transition metal oxides ( $\text{M}_x\text{O}_y$ ; M = Co, Fe, Ni, Cu, Mn, etc.) are considered feasible anode alternatives because of their high-specific capacities induced by conversion reaction mechanism, which was first proposed and elucidated by Poizot et al. [4]. This mechanism is characterized by the full reduction of transition metal oxides to nanograin metal particles embedded in the electrochemically reversible amorphous  $\text{Li}_2\text{O}$  matrix, which differs from the classical Li insertion/deinsertion or alloying/dealloying processes. Therefore, numerous studies have performed electrochemical evaluation of such transition metal oxides as cobalt oxides, iron oxides, nickel oxides, and copper oxides for application as the anode material in lithium-ion batteries [4–10].

In particular, many investigations have recently focused on nanostructure  $\text{Co}_3\text{O}_4$  as a promising anode alternative due to its higher theoretical capacity (890 mAh/g) compared to that of commercialized carbonaceous material (theoretical capacity: 392 mAh/g) which is now becoming limited owing to its low capacity. Extensive efforts have been made with the aim of achieving high electrochemical performances for lithium-ion batteries through the application of one-dimensional (1D)  $\text{Co}_3\text{O}_4$  nanowires [11, 12], nanostructured  $\text{Co}_3\text{O}_4$  thin films fabricated by electrochemical deposition method [13] or pulsed laser deposition [14], nanoparticulate  $\text{Co}_3\text{O}_4$  powders [15–17], and nanoparticle  $\text{Co}_3\text{O}_4$ /carbon composites [18, 19]. However, despite such efforts and the high reversible discharge and charge capacities, almost all nano-sized  $\text{Co}_3\text{O}_4$  systems exhibit unstable cycle characteristics upon cycling, and in

J.-G. Kang · Y.-D. Ko · J.-G. Park · D.-W. Kim (✉)  
Nano-materials Research Center, Nano-science Research  
Division, Korea Institute of Science and Technology,  
Seoul 136-791, South Korea  
e-mail: dongwan1@empal.com

particular suffer drastic capacity fading at a specific cycle number [11–13, 15, 17–19]. This detrimental phenomenon has been attributed to the aggregation of active nanograins [18], eventually leading to the electrical disconnection of active materials to current collector or conductive additives. Nevertheless, except for transmission electron microscopy (TEM) observations [15], few experimental approaches have been performed to examine this phenomenon in detail.

In this letter, we report on the simultaneous observation of variation in electrochemical impedance spectroscopy (EIS) data upon cycling, in order to examine the origin of the drastic capacity fading suffered in the nano-sized  $\text{Co}_3\text{O}_4$  anode system. In addition, the intimate association of cycling performance with the impedance elements in equivalent circuit analogs by fit experimental data is discussed.

## Experimental

$\text{Co}_3\text{O}_4$  nanopowders were prepared using the citrate-gel method. Anhydrous citric acid,  $\text{HOC}(\text{CH}_2\text{CO}_2\text{H})_2\cdot\text{CO}_2\text{H}$ , was added as the polymerization agent to  $\text{Co}(\text{NO}_3)_2\cdot 6\text{H}_2\text{O}$  dissolved in 1 L deionized water under stirring. The molar concentration of Co ions and the molar ratio of citric acid to Co ions were adjusted to 0.18 M and 1.333:1, respectively. The as-produced sol was dried at 100 °C in a vacuum oven to produce purple, rigid, glassy gels. These gels were calcined at 400 °C for 12 h in air atmosphere to obtain the crystalline  $\text{Co}_3\text{O}_4$  nanopowders.

The morphological and structural characteristics of the as-synthesized  $\text{Co}_3\text{O}_4$  powders were investigated using powder X-ray Diffraction (XRD, Model M18XHF, MacScience Instruments) pattern and TEM (Model JSM-6330F, JEOL). In addition, the lattice fringes in a  $\text{Co}_3\text{O}_4$  nanoparticle observed by high resolution TEM (HRTEM) were analyzed by means of fast Fourier transformation (FFT) method to acquire crystallographic information.

To prepare positive electrodes for the electrochemical tests, a mixture of 67 wt%  $\text{Co}_3\text{O}_4$  (2–3 mg) with 20 wt% Super P carbon black (MMM Carbon, Brussels, Belgium) and 13 wt% Kynar2801 binder (PVdF-HFP) dissolved in 1-methyl-2-pyrrolidinone (NMP) solvent was cast onto a Cu foil. After eliminating the solvent in a vacuum oven at 100 °C, Swagelok-type cells were assembled in an argon-filled glove box. The assembled cells consisted of  $\text{Co}_3\text{O}_4$ -based composites fabricated onto Cu foil as the positive electrode, Li metal foil as the negative electrode, and Celgard 2400 separator saturated with a 1 M  $\text{LiPF}_6$  electrolytic solution in 1:1 volume ratio of ethylene carbonate to dimethyl carbonate. The cells underwent cyclic voltammetry (CV) by collecting current signal with a

sweeping voltage (scan rate: 0.1 mV/s) over a range from 0.01 to 3.0 V in an electrochemical measurement unit (Solartron 1280C, UK). Furthermore, the assemble cells were galvanostatically cycled in the voltage window of 0.01–3.0 V at room temperature by means of an automatic battery cycler (WBCS 3000, WonATech, Korea).

To provide direct experimental evidence for the origin of the drastic decay of specific capacities from a certain point, EIS measurements were performed on the same unit (Solartron 1280C, UK). A lithium-ion half cell with an initial OCV over 3.0 V was galvanostatically ( $1\text{C} = 890 \text{ mA/g}$ ) discharged to 0.01 V, after which the impedance spectra were potentiostatically (0.01 V) obtained by imposing AC perturbation of 5 mV amplitude over the frequency range from 20 kHz to 1 mHz. Upon the following charge/discharge cycles, these sequential steps were repeated from the 10th to 100th discharged states at an interval of 10 cycles. For quantitative analysis, the data collected from the EIS measurement was curve-fitted by using Z-view software (version 2.90).

## Results and Discussions

The XRD pattern depicted in Fig. 1a is indicative of the formation of phase-pure  $\text{Co}_3\text{O}_4$  phase based on cubic spinel structure (space group:  $Fd\bar{3}m$ ), showing the main Bragg's reflection peak in the (311) plane. Moreover, analysis of the (311) peak with the Scherrer equation,  $D = 0.94\lambda/(B \cos \theta)$ , indicated that the primary particle size of the  $\text{Co}_3\text{O}_4$  nanopowders was approximately 20 nm ( $D$ : average dimension of crystallites,  $\lambda$ : wavelength of X-ray,  $B$ : full width at half maximum of a reflection located at  $2\theta$ ). Spherical nanoparticulate morphology with an average particle size from 20 to 30 nm was identified in Fig. 1b and c, which is in good agreement with result calculated by the Scherrer equation. In addition, the high crystallinity of these nanoparticles was clearly evident in the HRTEM lattice fringes of the  $\text{Co}_3\text{O}_4$  nanoparticle in the magnifying square region in Fig. 1c, as shown in Fig. 1d. The measured lattice spacings in the FFT pattern of Fig. 1e also supported the formation of the  $\text{Co}_3\text{O}_4$  phase.

The galvanostatic cycling characteristics of nano-sized  $\text{Co}_3\text{O}_4$  powders in the configuration of the  $\text{Co}_3\text{O}_4/\text{Li}$  half cell were investigated over the 0.01–3.0 V voltage window at a rate of  $C/5$  ( $=178 \text{ mA/g}$ ) during 100 cycles. In the charge/discharge voltage profiles in Fig. 2a, a long voltage plateau appears near 1.05 V, in association with the conversion reaction of  $\text{Co}_3\text{O}_4$  to Co and  $\text{Li}_2\text{O}$  ( $\text{Co}_3\text{O}_4 \rightarrow 3\text{Co} + 4\text{Li}_2\text{O}$ ). The following sloping part, where the cell is reduced from 1.05 V down to 0.01 V, leads to the evolution of an extra capacity due to the formation of Li-bearing gel-like polymeric layers [7]. The variation of the discharge

**Fig. 1** **a** XRD pattern of nano-sized  $\text{Co}_3\text{O}_4$  with cubic spinel structure, **b** and **c** typical low-magnification images of nano-sized  $\text{Co}_3\text{O}_4$ , **d** magnified HRTEM images of a selected region in **c**, and **e** FFT pattern calculated from a single  $\text{Co}_3\text{O}_4$  nanoparticle

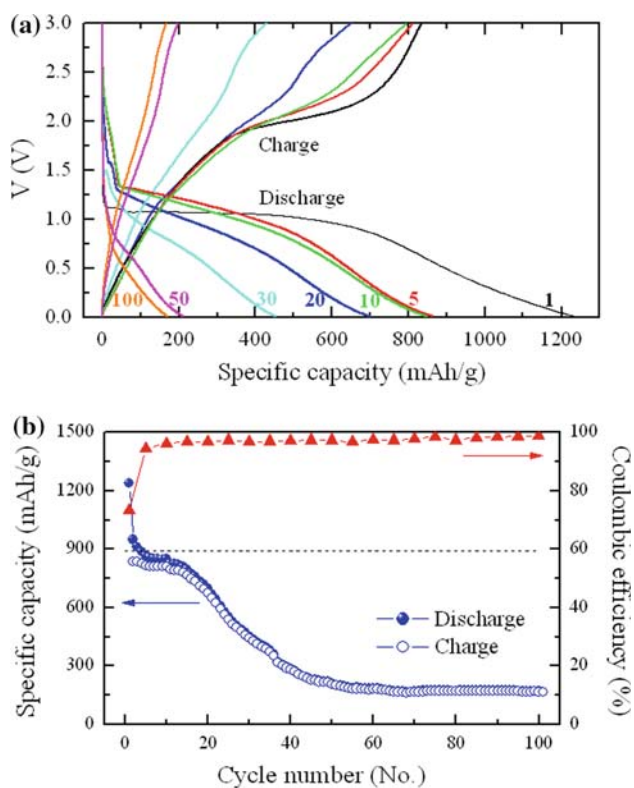
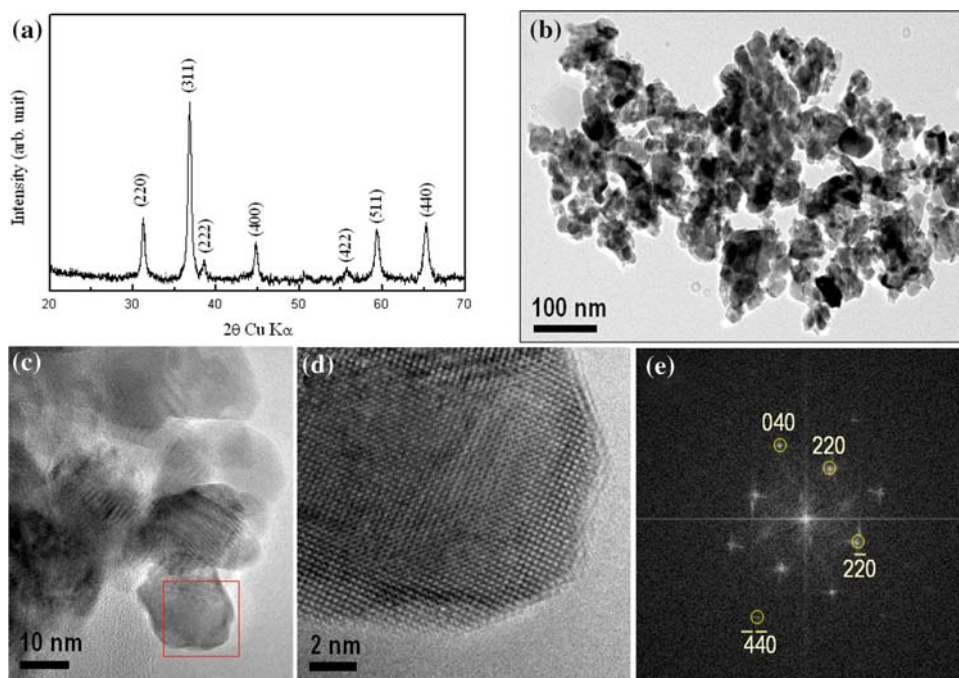


**Fig. 2** Galvanostatic electrochemical evaluation of nano-sized  $\text{Co}_3\text{O}_4/\text{Li}$  half-cell at a rate of  $C/5$  during 100 cycles: **a** discharge/charge voltage profiles between 0.01 and 3.0 V at a rate of  $C/5$ , and **b** plot of discharge/charge capacities against cycle number. The closed and open circular symbols denote the discharge and charge capacities, respectively. The closed triangular symbol indicates coulombic efficiency

and charge capacities with cycle number is exhibited in Fig. 2b, along with the theoretical capacity (890 mAh/g, dotted line). The first discharge and charge capacities were 1237 and 835 mAh/g, respectively, indicating a coulombic efficiency of 73%. The capacity loss may have resulted from the formation of a solid electrolyte interface (SEI) layer due to electrolyte decomposition. The electrochemical cycling of nano-sized  $\text{Co}_3\text{O}_4$  was stable for the initial 20 cycles, with the capacity being maintained close to the theoretical capacity. However, Fig. 2b shows the drastic capacity fading from the 20th cycle, suggesting a drastic loss in the electrochemical activity for the  $\text{Co}_3\text{O}_4$  electrode.

The family of Nyquist plots at each discharged state is presented in Fig. 3a, with the data collected from high to medium frequency ranges (20 kHz–10 Hz). An electrochemical process typically involves various reactions or steps such as lithium-ion conduction inside SEI layers, charge transfer at the SEI layers/electrolyte interface (electrical double layer), electronic conduction through the bulk composite electrode, solid-state diffusion, and pseudo-capacitive behavior due to charge accumulation inside the particle [20–22]. As the relaxation time constant is specific to each individual reaction, the variation of each constant among different reaction can be separated by sweeping an AC frequency signal if a resolvable difference is detected among them. From this point of view, two distinctive, depressed semicircular arcs (not fully developed arc in Section II due to high frequency limitation) can be observed in the inset of Fig. 3a (20th cycle). Although modeling of this impedance spectra by equivalent circuit analogs usually introduces vagueness at low frequency

ranges, including Warburg diffusive and pseudo-capacitive components, quantitative analysis can be performed by using the generally accepted equivalent circuit at high-to-medium frequency ranges, as depicted in the inset of Fig. 3a.

An equivalent circuit is made up of a serial connection of (I)  $R_{el}$ , (II)  $R_{sei}/CPE_{sei}$  ( $CPE_{sei}$  parallel to  $R_{sei}$ ), and (III)  $R_{ct}/CPE_{dl}$ , which represent the ionic resistance of the

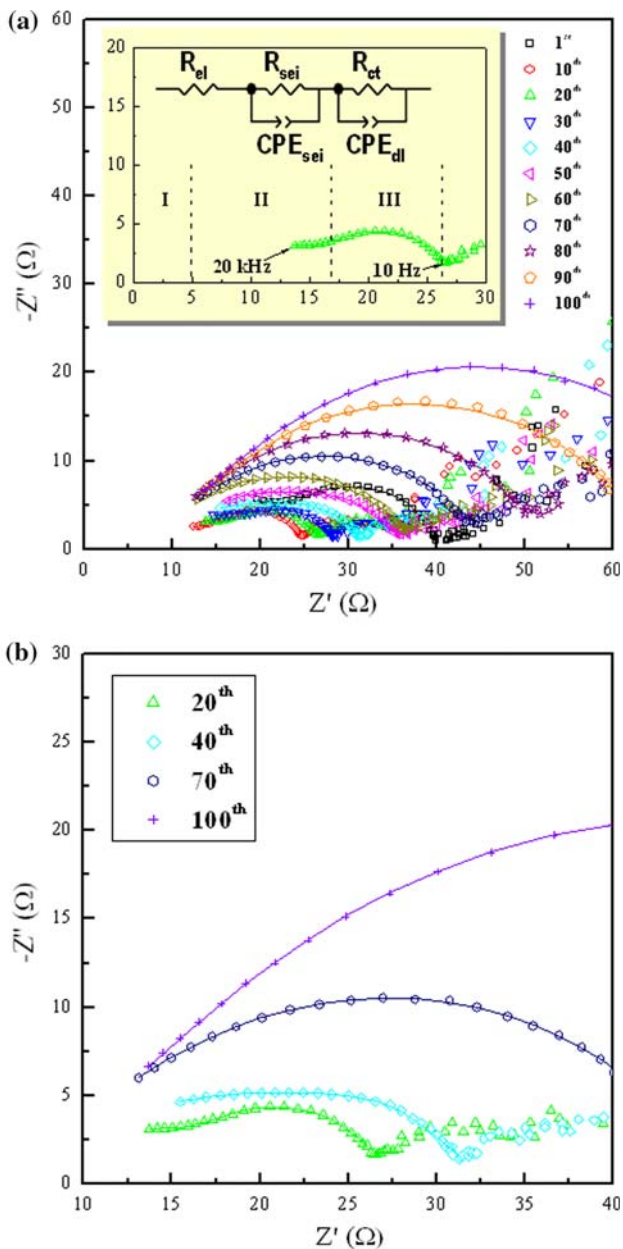


**Fig. 3** **a** Family of Nyquist plots collected from the 1st and 10th–100th discharged states (at 10-cycle intervals) over a frequency range from 20 kHz to 10 Hz, including an equivalent circuit analog for curve fitting. **b** Magnified view of Nyquist plots for the 20th, 40th, 70th, and 100th discharged states to show the disappearance of the border between SEI and charge transfer contribution

electrolyte, ionic conduction inside the SEI layers, and charge transfer reaction at the electrode/electrolyte interface, respectively.  $R_i$  denotes the resistance of each process and constant phase element ( $CPE_i$ ) stands for the capacitance, rather than the pure capacitance ( $C$ ), in order to reflect the non-homogeneous nature of the porous composite electrode, resulting in a depressed semicircular shape [23, 24]. By curve fitting of the Nyquist plots with this circuit model, we obtained reliable quantitative values of each circuit element supported by chi-square ( $\chi^2$ ) of the order of  $10^{-5}$ – $10^{-4}$ . Furthermore, both semicircles increased with increasing cycle number, as shown in Fig. 3b in detail. This indicated that lithium-ion conduction inside the SEI layers and charge transfer at the electrode/electrolyte interface became hindered upon subsequent cycles. As can be seen, the distinctive feature of two semicircles began to vanish from the 40th cycle, eventually transforming to one semi-circle-like characteristic. This result may have arisen from the evolution of indistinguishable relaxation times between the two processes since the resistive components of both reactions gradually increase.

By curve-fitting Nyquist plots in Fig. 3 for quantitative analysis, the variation of  $R_{sei}$  and  $R_{ct}$  during cycling was obtained (Fig. 4). The  $R_{sei}$  values, as a measure of the hindrance for lithium-ion conduction through the SEI layers, slightly decreased in the initial 50 cycles but then rapidly increased in the following cycles. This behavior is indicative of the stabilization of SEI layers achieved during the initial 50 cycles, which does not support the sudden decay of capacity from the 20th cycle with  $R_{sei}$ . Interestingly,  $R_{ct}$  dramatically increased as the cycling continued from the 20th cycle. Considering that the charge transfer at the electrode/electrolyte interface is usually interpreted as the reaction expressed by the Butler–Volmer type equation [25, 26], the sudden change in feasible processes involved in

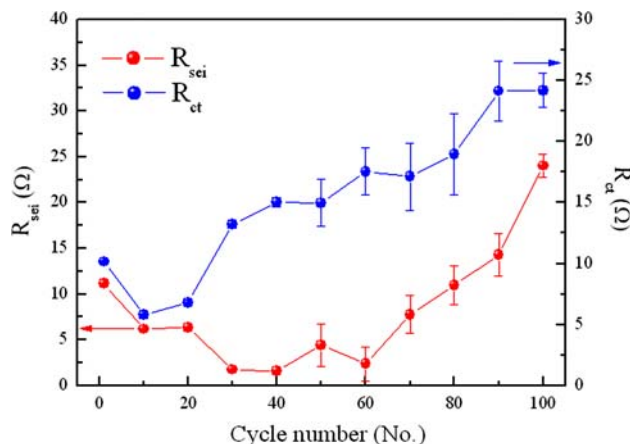


**Fig. 4** The resistive components of SEI and charge transfer reaction according to the cycle number, as calculated from previous Nyquist plots by curve fitting

charge transfer as the partial desolvation reaction, adsorption, and surface diffusion of lithium-ions on the electrode surface are postulated as the origins of the drastic capacity fading. Nano-sized electrode materials offer good charge transfer kinetics due to their shorter path lengths. However,  $\text{Co}_3\text{O}_4$  materials undergo a large volume change of around 100% due to the electrochemical conversion reaction, thereby introducing mechanical stress and subsequent microstructural failure that prevent efficient electronic conductive paths and increase the charge transfer resistance [7]. As mentioned earlier, the charge transfer resistance should be increased by the hindrance to charge transfer reaction at the electrode/electrolyte interface. Indeed, the increase in internal defects and isolated active regions which hardly react with the electrolyte can increase the charge transfer resistance during continued cycling in nano-sized  $\text{Co}_3\text{O}_4$  electrodes. Here, the trend in charge transfer resistance was in good agreement with the charge and discharge capacity behavior upon cycling shown in Fig. 2b. Therefore, the origin of drastic capacity decay was attributed to the increase in charge transfer resistance of the  $\text{Co}_3\text{O}_4$  electrodes, i.e., the suppression of reaction between Li-ions and electrons at the electrode/electrolyte interface upon cycling.

## Conclusion

In the present work,  $\text{Co}_3\text{O}_4$  nanopowders were successfully synthesized using the citrate-gel method. The XRD patterns and TEM results demonstrated the formation of a cubic spinel  $\text{Co}_3\text{O}_4$  material with homogeneous particle size (average size: 20–30 nm). Using powerful AC EIS analysis, we demonstrated unstable cycle features, drastic capacity fading in nano-sized  $\text{Co}_3\text{O}_4$ , and the variation of resistive components (SEI layers and charge transfer) according to the cycle number. In addition, we clearly ascertained the direct association of charge transfer resistance with capacity fading features. Although further analytical study based on AC impedance needs to be performed in order to reveal the full complexity of this issue, the present study results have illuminated the applicability of various new approaches for examining the cycling stability performances of other electrochemical conversion electrode materials.

## References

- J.M. Tarascon, M. Armand, *Nature* **414**, 359 (2001). doi:[10.1038/35104644](https://doi.org/10.1038/35104644)
- A.S. Arico, P. Bruce, B. Scrosati, J.M. Tarascon, W.V. Schalkwijk, *Nat. Mater.* **4**, 366 (2005). doi:[10.1038/nmat1368](https://doi.org/10.1038/nmat1368)
- C. Jiang, E. Hosono, H. Zhou, *Nanotoday* **1**, 28 (2006)
- P. Poizot, S. Laruelle, S. Grugeon, L. Dupont, J.M. Tarascon, *Nature* **407**, 496 (2000). doi:[10.1038/35035045](https://doi.org/10.1038/35035045)
- D. Larcher, G. Sudant, J.B. Leriche, Y. Chabre, J.M. Tarascon, *J. Electrochem. Soc.* **149**, A234 (2002). doi:[10.1149/1.1435358](https://doi.org/10.1149/1.1435358)
- S. Grugeon, S. Laruelle, R. Herrea-Urbina, L. Dupont, P. Poizot, *J. Electrochem. Soc.* **148**, A285 (2001). doi:[10.1149/1.1353566](https://doi.org/10.1149/1.1353566)
- S. Laruelle, S. Grugeon, P. Poizot, M. Dolle, L. Dupont, J.M. Tarascon, *J. Electrochem. Soc.* **149**, A627 (2002). doi:[10.1149/1.1467947](https://doi.org/10.1149/1.1467947)
- D. Larcher, D. Bonnin, R. Cortes, I. Rivals, L. Personnaz, J.M. Tarascon, *J. Electrochem. Soc.* **150**, A1643 (2003). doi:[10.1149/1.1622959](https://doi.org/10.1149/1.1622959)
- A. Debart, L. Dupont, P. Poizot, J.B. Leriche, J.M. Tarascon, *J. Electrochem. Soc.* **148**, A1266 (2001). doi:[10.1149/1.1409971](https://doi.org/10.1149/1.1409971)
- D. Larcher, C. Masquelier, D. Bonnin, Y. Charbre, V. Masson, J.B. Leriche et al., *J. Electrochem. Soc.* **150**, A133 (2003). doi:[10.1149/1.1528941](https://doi.org/10.1149/1.1528941)
- K.T. Nam, D.W. Kim, P.J. Yoo, C.Y. Chiang, N. Meethong, P.T. Hammond et al., *Science* **312**, 885 (2006). doi:[10.1126/science.1122716](https://doi.org/10.1126/science.1122716)
- K.M. Shaju, F. Jiao, A. Debart, P.G. Bruce, *Phys. Chem. Chem. Phys.* **9**, 1837 (2007). doi:[10.1039/b617519h](https://doi.org/10.1039/b617519h)
- S.L. Chou, J.Z. Wang, H.K. Liu, S.X. Dou, *J. Power Sources* **182**, 359 (2008). doi:[10.1016/j.jpowsour.2008.03.083](https://doi.org/10.1016/j.jpowsour.2008.03.083)
- V. Pralong, J.B. Leriche, B. Beaudoin, E. Naudin, M. Mocrete, J.M. Tarascon, *Solid State Ion.* **166**, 295 (2004). doi:[10.1016/j.ssi.2003.11.018](https://doi.org/10.1016/j.ssi.2003.11.018)
- S. Grugeon, S. Laruelle, L. Dupont, J.M. Tarascon, *Solid State Sci.* **5**, 895 (2003). doi:[10.1016/S1293-2558\(03\)00114-6](https://doi.org/10.1016/S1293-2558(03)00114-6)
- X. Wang, X. Chen, L. Gao, H. Zheng, Z. Zhang, Y. Qian, *J. Phys. Chem. B* **108**, 16401 (2004). doi:[10.1021/jp048016p](https://doi.org/10.1021/jp048016p)
- G.X. Wang, Y. Chen, K. Konstantinov, J. Yao, J.H. Ahn, H.K. Liu, S.X. Dou, *J. Alloy Comp.* **340**, L5 (2002). doi:[10.1016/S0925-8388\(02\)00005-1](https://doi.org/10.1016/S0925-8388(02)00005-1)
- R. Yang, Z. Wang, J. Liu, L. Chen, *Electrochem. Solid-State Lett.* **7**, A496 (2004). doi:[10.1149/1.1819861](https://doi.org/10.1149/1.1819861)
- S.A. Needham, G.X. Wang, K. Konstantinov, Y. Tournayre, Z. Lao, H.K. Liu, *Electrochem. Solid-State Lett.* **9**, A315 (2006). doi:[10.1149/1.2197108](https://doi.org/10.1149/1.2197108)
- J.R. Macdonald, *Impedance Spectroscopy; Theory, Experiment, and Applications*, 2nd edn. (Wiley, New York, 2005), pp. 444–446
- M.D. Levi, D. Aurbach, *J. Phys. Chem. B* **101**, 4630 (1997). doi:[10.1021/jp9701909](https://doi.org/10.1021/jp9701909)
- S. Kobayashi, Y. Uchimoto, *J. Phys. Chem. B* **109**, 13322 (2005). doi:[10.1021/jp044283j](https://doi.org/10.1021/jp044283j)
- P. Yu, J.A. Ritter, R.E. White, B.N. Popov, *J. Electrochem. Soc.* **147**, 2081 (2000). doi:[10.1149/1.1393489](https://doi.org/10.1149/1.1393489)
- N. Sharma, G.V. Subba Rao, B.V.R. Chowdari, *Electrochim. Acta* **50**, 5305 (2005)
- M. Nakayama, H. Ikuta, Y. Uchimoto, M. Wakihara, *J. Phys. Chem. B* **107**, 10603 (2003). doi:[10.1021/jp036059k](https://doi.org/10.1021/jp036059k)
- S. Kobayashi, Y. Uchimoto, *J. Phys. Chem. B* **109**, 13322 (2005). doi:[10.1021/jp044283j](https://doi.org/10.1021/jp044283j)